ULF Modulations on Plasma Environment and Coherent Waves of Mercury's Magnetosphere: MESSENGER's Observation

J. -T. Zhao[1], Q. -G. Zong[1], C. Yue[1], X. -Z. Zhou[1], Z. -Y. Liu[1], W. -J. Sun[2], J. A. Slavin[2], J. M. Raines[2], X. -Y. Zhu[1]

[1]School of Earth and Space Sciences, Peking University, Beijing 100871, China.
[2]Department of Climate and Space Sciences and Engineering, University of Michigan, Ann Arbor, Michigan 48109, USA.

Key Points:

- ∼15 mHz magnetic field pulsations were detected and found to be capable of driving proton flux fluctuations in Mercury's magnetosphere.
- The associated ∼1 Hz magnetic waves have ∼15 mHz variations in power and compressibility, indicating modulation by the ∼15 mHz compressional waves.
- The influence on ∼1 Hz waves is possibly attained by plasma flux changes, helping us better interpret its wave mode and character.

Corresponding author: Q. -G. Zong, qgzong@pku.edu.cn

Abstract

Ultra low-frequency (ULF) waves are fundamental waves that can energize, transport, and scatter charged particles in planetary magnetospheres. With the measurements from MErcury Surface, Space ENvironment, GEochemistry, and Ranging (MESSENGER), we investigate the proton flux fluctuations and coherent waves associated with a series of ULF waves on the flanks of Mercury's magnetosphere. The ULF waves are mainly compressional with a frequency of ∼15 mHz and significantly modulate the intensity of proton flux. The coherent waves accompanied by the ULF waves correspond to a higher frequency (∼1 Hz). The wave power and compressibility of the coherent waves vary quasi-periodically with the ∼15 mHz ULF waves. We conclude that the compressional ULF waves modulate the coherent waves with higher frequency. This modulation might result from the associated periodic proton flux changes and helps us understand the nature of the ∼1 Hz waves better.

Plain Language Summary

This study presents MESSENGER observations of wave-particle interactions on the flank of Mercury's magnetosphere. Clear one-to-one modulation of proton flux by ∼15 mHz compressional waves is shown in these two cases. Proton gyro-frequency (∼1 Hz) waves are observed during the same interval. Their amplitudes and compressibilities are periodic with a frequency of ∼15 mHz, coinciding with the frequency of the compressional waves. This coincidence indicates that the ∼1 Hz waves are possibly affected by the ∼15 mHz waves. The above observational facts demonstrate that ULF waves can modify the plasma environment and further affect the kinetic scale dynamics in the magnetosphere of Mercury. Its importance is further validated by our statistical result, which shows that wave-particle and wave-wave modulation are not rare events.

1 Introduction

As the innermost and the smallest planet in the solar system, Mercury has a dipole moment of 190 $nT \cdot R_M^3$ with the dipole center shifting northward by 0.2 R_M (R_M refers to Mercury's radius, which equals to 2440 km) from the geographic center (Alexeev et al., 2010; Anderson et al., 2011, 2012). Due to strong solar wind enforcement, a highly compressed magnetosphere with an average magnetopause subsolar distance of ∼ 1.45 R_M forms (Slavin et al., 2009; Winslow et al., 2013; Philpott et al., 2020). Mercury has a series of magnetospheric structures (e.g. polar cusp, magnetotail plasma sheet, plasma mantle) and substorm activities (e.g., dipolarization, flux rope) that are similar to those of Earth (Raines et al., 2011; Gershman et al., 2014; Sun, Slavin, Fu, Raines, Zong, et al., 2015; DiBraccio et al., 2015; Imber & Slavin, 2017; Zhao et al., 2019). Recent observation study reports that Mercury also has a ring current that consist of ∼ keV proton within the magnetosphere (Zhao et al., 2022). Apart from these structures and activities, magnetohydrodynamic and plasma waves have also been reported and investigated in previous studies (e.g., Sundberg et al., 2012; Boardsen et al., 2012, 2015; Kim et al., 2016).

Ultra-low frequency (ULF) pulsations are one of the most common waves in space plasma (Jacobs & Westphal, 1964). They play essential roles in both the magnetosphere and solar wind. These waves are efficient mediums for energy transport (e.g., fast mode magnetosonic waves at the arrival of interplanetary shock (Q.-G. Zong et al., 2009)). Fluctuating electromagnetic fields can directly change the energy and momentum of charged particles and result in modulation, energization, transport, and loss of charged particles (Elkington et al., 2003; Q.-G. Zong et al., 2009; Loto'aniu et al., 2010; Yue et al., 2016; Q. Zong et al., 2017; Z.-Y. Liu et al., 2020). These changes in charged particles may further influence the amplitudes and propagations of the original waves or excite other types of waves (Kim et al., 2016; S. Liu et al., 2019).

ULF pulsations near Mercury have been investigated by the observation of Mariner 10 and MESSENGER. The earliest study can be traced back to a Mariner 10 observation of ∼0.5 Hz linearly polarized magnetic field fluctuations with both compressional and transverse modes (C. T. Russell, 1989). The similar type of waves is further investigated through MESSENGER observations (e.g., Boardsen et al., 2012, 2015; Kim et al., 2016). Based on two years of observations from MESSENGER, Boardsen et al. (2012) statistically analyzed and quantified the characteristics of these waves. The frequency ranges from 0.4 Hz to 5 Hz, approaching the local proton gyro-frequency. These waves are more likely to occur at the duskside rather than at the dawnside. They have the maximum occurrence rate near the radial distance of ∼1.4 R_M around the magnetic equator. These waves tend to be transverse in the higher magnetic latitudes and tend to be compressional near the magnetic equator. These transverse dominant waves (ratio of transverse power to total power > 0.7) are linearly polarized at higher magnetic latitudes. Some of these waves have up to at least fourth harmonics.

Several studies proposed that these ∼1 Hz waves may be generated via ion-ion hybrid resonance since the contribution of heavy ions in Mercury's magnetosphere is significant (e.g., Kim et al., 2016). In addition, the observed compressional component can be converted from the transverse component via mode conversion. However, from MESSENGER's observation, the compressional mode is always dominant ($\delta B_{\parallel}^2 > \delta B_{\perp}^2$ for 75% wave events), which does not support the ion-ion hybrid resonance hypothesis (Boardsen et al., 2012; Kim et al., 2016). Such compressible waves that concentrated near the magnetic equator were interpreted as another mode, electromagnetic ion Bernstein mode waves (Boardsen et al., 2015). The electromagnetic ion Bernstein mode waves exhibit large compressibility in high beta plasma (Denton et al., 2010; Boardsen et al., 2015). Moreover, ray tracing simulation (Rönnmark & André, 1991; Boardsen et al., 2015) shows that these electromagnetic ion Bernstein mode waves propagate between the magnetic latitude of ±12°, which explains the latitudinal difference in wave compressibility.

Long-period (minute-period, ∼15 mHz, or ∼60 s) waves were also examined from MESSENGER's measurements. Boardsen et al. (2010) and Sundberg et al. (2012) first reported minute-period Kelvin-Helmholtz (KH) pulsations at Mercury's magnetopause with comprehensive analysis of both the magnetic field and plasma. These KH waves are found to drive large amplitude ∼15 mHz waves inside the magnetosphere (Liljeblad et al., 2016). James et al. (2019) proposed that some of these ∼15 mHz waves are generated via field line resonance because they have a dominant toroidal component and reversal of handedness. In a study on the nightside plasma sheet, MESSENGER observed series of plasma waves with period of 10 to 20 s, which are near circularly polarized in the high magnetic latitude and are compressional waves near the magnetic equator (Sun, Slavin, Fu, Raines, Sundberg, et al., 2015).

However, the influence of these magnetospheric waves on the plasma has not been well investigated in Mercury's magnetosphere, which was partly due to the field-of-view (FOV) limitation of MESSENGER's ion measurements. There is still no measurements on the direct modulations between waves of different frequencies. In this study, we report two cases of proton flux fluctuations modulated by ∼15 mHz compressional waves observed by the MESSENGER spacecraft. Coherent ∼1 Hz waves are also present simultaneously in these events. Their power and compressibility are correlated with the ∼15 mHz waves. Moreover, our statistical research verifies that the ∼15 mHz wave modulations on proton flux and high-frequency waves are commonly observed and noteworthy. The paper is organized as follows: First, we will show two case studies: including an overview of the wave events and detailed analyses from both magnetic field and particle views. Then follow the statistics on the ∼15 mHz wave modulations covering two Mercury years. The possible wave mode and explanations for the observed modulation are discussed in the following section. Finally, we will summarize the observations and inferences of this study.

2 Result

2.1 Case I: 19th March, 2014

On 19th March, 2014, MESSENGER's magnetometer (MAG) (Anderson et al., 2007) detected periodic magnetic field fluctuations with a period of ∼64 s (i.e. ∼15 mHz) in the duskside magnetosphere of Mercury. The first two panels in Figure 1 show the 46 eV to 13.3 keV energy spectrum and pitch angle distribution of protons measured by the fast imaging plasma spectrometer (FIPS) with 10 s resolution (Andrews et al., 2007). Figure 1c shows the magnetic field vectors with 20 Hz resolution, and Figure 1d shows the magnetic latitude and magnetic local time of MESSENGER. The average energy spectrum during the time interval of interest(UT 10:30 - UT 10:42) is shown as red crosses in Figure 1e. Figure 1f displays the average pitch angle distribution of proton within this interval. MESSENGER's trajectory is presented in Figures 1g and 1h. The time interval of interest is marked by the gray shadow region and bold gray line in Figures 1a-1d and 1g-1h, respectively. The coordinate system used here is the aberrated Mercury Solar Magnetospheric coordinate system (aMSM). In this coordinate system, the X-axis is antiparallel to the solar wind inflow direction (assuming that the solar wind speed is 400 km/s and radial outward). The Z-axis points to Mercury's geographic north pole. The orientation of the Y-axis can be determined by their cross product (i.e. $\vec{\mathbf{e}}_\mathbf{y} = \vec{\mathbf{e}}_\mathbf{z} \times \vec{\mathbf{e}}_\mathbf{x}$). The coordinate system's center deviates from Mercury's geographical center 0.2 R_M northwardly due to the off-centered dipole field (Anderson et al., 2011).

During this interval, MESSENGER moves equatorward from Northern Hemisphere within the meridian plane of ∼18 h local time. The magnetic field direction changes from dawnward to northward, and the strength decreases gradually as the spacecraft moves toward the equator. The increasing signature in the proton flux coincides with the previous statistics about the background proton distribution (Zhao et al., 2022). The absence of the protons with a pitch angle of $\sim 180°$ can be seen in Figure 2b, while the conjugate proton with a pitch angle of $\sim 0°$ is not measurable due to the limited field of view of FIPS. The ∼64 s periodic fluctuations with ∼10 nT amplitude appear in the magnetic field observations between UT 10:30 and UT 10:40. Such ∼64 s periodic variation also exists in the proton energy spectrum of Figure 1a and pitch angle spectrum of Figure 1b. The magnetic field and proton flux fluctuate irregularly after UT 10:48, implying that the spacecraft enters the magnetosheath. As the proton energy spectrum and pitch angle spectrum do not vary much during this interval, we averaged the proton energy spectrum (Figure 1e) and pitch angle spectrum (Figure 1f) within the time of interest to improve signal to noise ratio.The average energy spectrum shown in Figure 1e greatly exceeds the one-count level except for the low-energy range (<0.12 keV, the left gray dashed line) and high-energy tail (> 4.7 keV, the right gray dashed line), which means that the proton distributions with energies between the low- and high-energy ends are reliable. The average pitch angle spectrum shown in Figure 1f presents an anisotropic pitch angle distribution. The parallel (0°-10°) and anti-parallel ($150° - 180°$) pitch angle bins are highly uncertain (the standard error of the mean flux exceeds the 50% of the mean flux) and shown as red bins in the integrated pitch angle distribution.

The proton energy spectrum during the interval with substantial wave activity is presented in Figure 2a. The integrated proton flux within the reliable energy range (0.12 keV to 4.7 keV) is presented as the solid black line, revealing an obvious periodic variation. Pitch angle distributions shown in Figure 2b demonstrates that the periodic variation is almost pitch-angle independent. The magnetic pulsation signals, after subtracting a moving-averaged B field with a window of 300 s, are shown in Figure 2c. Here, the residual magnetic field vectors are transformed into the field-aligned coordinate system. In this coordinate system, the compressional component ($\delta B_\parallel$) is parallel to the local magnetic field, and the poloidal and toroidal components (δB_{po} and δB_{to}) point outward and eastward along the normal plane of the local magnetic field, respectively. The pulsations consist of compressional, toroidal, and poloidal modes. Panel d presents the wavelet spec-

trum of the detrended compressional mode signal. The governing component has a period of ∼64 s, and the secondary component locates around the period of ∼36 s, which is close to the second harmonic period. The power of ∼36 s fluctuations increases rapidly at UT 10:40 as the ∼64 s component gradually decreases. Here, we focus on the observation of monochromatic ∼64 s waves with clear proton modulation before UT 10:40.

In addition, ∼1 Hz waves are detected during this interval. These waves are analyzed by the singular value decomposition technique described in Santolík et al. (2003) and Boardsen et al. (2015). Figures 3a and 3b present the power spectrum density derived from wavelet analysis. The solid white line in each panel indicates the proton gyro-frequency. The wave power is mainly concentrated at constant frequencies between 0.5 Hz and 2.0 Hz, close to the proton gyro-frequency. The transverse components are the dominant components, and the compressional component becomes comparable as the spacecraft approaches the magnetic equator. Meanwhile, the total wave power increases. Ellipticity and coherence analyses are presented in Figures 3c and 3d. The low ellipticity and high coherence characteristics of these waves are consistent with the observational characteristics of the waves investigated in Boardsen et al. (2015). The waveforms detrended from the 5 s moving average magnetic field are presented in Figure 3e, showing a difference in wave power at different latitudes. Apart from the latitudinal variations, periodic wave power and components can also be seen, which are likely associated with the ∼15 mHz waves. Here we select three time slices with large amplitude ∼1 Hz waves and show their zoomed-in waveforms in the bottom three panels (Figures 3f-h). These waveforms demonstrate that the ∼1 Hz waves have different amplitudes, compressibility, and frequency bandwidth at different times.

Here, we focus on the five periods of ∼15 mHz waves from UT 10:31:30 to UT 10:39:00 with clear modulation of the ∼1 Hz waves. Figures 4a, 4b, and 4c are adapted from Figures 2a, 2c, and 3e to show the proton energy spectrum, the ∼15 mHz wave signal, and the ∼ 1 Hz wave signal. Integral wave power within 0.5 Hz to 2 Hz is presented in Figure 4d. The compressional and transverse mode power time series are plotted as solid red and blue lines, respectively. We use compressibility (i.e., the ratio of compressional mode and total power) to quantify the wave mode, as shown in Figure 4e. There are one-to-one correspondences between the ∼15 mHz compressional mode wave dips (Figure 4b) and ∼1 Hz wave compressibility peaks. In addition, the integral power of the ∼1 Hz waves (Figure 4d) also seems to be modulated by the ∼15 mHz compressional waves, although their one-to-one correspondences are not very distinct. The integral wave power and compressibility are Fourier transformed to explore their temporal variation. The results shown in Figure 4f demonstrate that they vary with a common period of ∼64 s, coinciding with the frequency of long-period $\delta B_{\parallel}$ and 0.12 keV to 4.7 keV proton flux variations observed during the same interval. Additional power density peaks at approximately ∼1/36 Hz are shown in the dynamic spectrum of the ∼1 Hz wave power and compressibility.

2.2 Case II: 4th July, 2013

On 4th July 2013, MESSENGER detected another ULF waves-proton modulation event (Figure 5, in the same format as Figure 1) in the dawnside flank region. Apparent magnetic field perturbation can be seen between UT 00:22 and UT 00:30 (Figure 5c). We adopted the same method used in Case I to analyze this event. The proton energy spectrum (Figure 5a) and pitch angle spectrum (Figure 5b) do not present abrupt changes during this interval. The averaged proton energy spectrum presented in Figure 5e reveals a significant count within 0.2 keV and 8.4 keV and maximum counts around ∼1 keV. And the averaged pitch angle spectrum shown in Figure 5f indicates an even larger anisotropy than the first case. The background magnetic field is about 100 nT and dominated by the northward component. This event is observed at no more than 15° mag-

netic latitudes (Figure 5d). As the spacecraft moves out of the equator (Figures 5g,h), the observed proton flux decrease, and the magnetic field intensity increase.

The proton modulation analysis is presented in Figure 6. Panels a, b, c, and d show the zoom-in proton energy spectrum, pitch angle spectrum, detrended magnetic field, and compressional wavelet spectrum. Five one-to-one correspondences between compressional ULF waves and integral proton fluxes are observed in this event. The magnetic field fluctuations have amplitudes $\sim$ 5 nT and are mainly contributed by the compressional component. The wavelet spectrum suggests the wave periods are 90 s and 55 s (11 and 18 mHz, $\sim$15 mHz) at the magnetic equator and higher magnetic latitude. Compared to the first case, the ULF wave amplitudes are lower, and the transverse components are negligible to the compressional component. The proton flux fluctuations are also less significant.

Proton-gyro frequency waves are observed within the same duration. Figures 7a and 7b show the compressional and transverse power spectra within this duration, respectively. The proton gyro-frequency is shown as the solid white line in both panels. The second harmonic waves around $\sim$2-3 Hz are revealed between UT 00:25-00:30. Ellipticity and coherence spectrum are presented in the following c, d panels. The detrended waveforms shown in Figure 7e suggest both the overall increasing trend and periodic fluctuations of the compressional and transverse wave amplitudes as the spacecraft moves poleward. Also, both waves tend to be monochromatic at higher magnetic latitudes and broadband around the equator. These waves present constant central frequency, low ellipticity, and high coherence. These characteristics are coincident with the first case. Figures 7f, g, and h present three exampled waveforms during this event. Unlike the first case, the compressional mode waves are always dominant.

Figure 8 shows the modulation relationship between the compressional long-period ULF waves, proton flux, and short-period wave powers. It should be noted that the long-period ULF waves do not modulate the $\sim$ 1 Hz wave compressibility in this case. The lack of compressibility modulation indicates that long-period ULF waves might not be sufficient to drive perturbation of proton flux and high-frequency waves every time. A statistical investigation is required to confirm the long-period ULF waves' common influence on particles and high-frequency waves.

2.3 Statiscial Result

The above cases reveal similar observational characteristics: The long-period ULF waves modulate proton flux and short-period ULF wave power. To understand the importance and role of the ULF waves, we furtherly investigate another 142 long-period ULF wave cases from 1st July 2013 to 30th September 2013 and from 1st January 2014 to 31st March 2014 (consisting of 546 MESSENGER orbits, $\sim$2 Mercury years). These ULF waves have periods between 30 - 120 s, durations longer than three wave periods, and an amplitude larger than 1 nT. The case list is shown in the Supporting Information(SI). Among the 142 cases, 63 present modulation (at least three wave periods with one-to-one correspondences). 31 of the 63 proton-modulation cases and 16 of the 79 non-proton-modulation cases reveal high-frequency waves with power modulated by the long period ULF waves. These results imply that the long-period ULF waves-proton flux modulation and long-period ULF waves-short period ULF wave modulation occur with considerable frequencies in Mercury's magnetosphere.

3 Discussion and Summary

Although we cannot determine the exact wave modes of the $\sim$1 Hz waves and $\sim$15 mHz waves, our observations provide some pieces of evidence to diagnose the wave property.

The ∼15 mHz compressional waves play the most crucial role in this event. Their frequency is much lower than the proton gyro-frequency and ∼2 times lower than the Na^+ gyro-frequency. Compared to the frequency (∼ several Hz) of ion-ion hybrid resonance and electromagnetic ion Bernstein mode waves (Kim et al., 2016; Boardsen et al., 2015), the frequency of ∼15 mHz is much lower. Therefore, these waves are more likely magnetohydrodynamic waves than kinetic plasma waves. According to the out-of-phase correlation between proton flux and compressional component of magnetic field, slow mode magnetosonic waves and drift mirror mode waves are two possible candidates for the observed ∼15 mHz waves. For slow magnetosonic waves, the thermal pressure gradient force and magnetic pressure gradient force are out-of-phase coupled and contribute to the restoring force together, naturally explaining the one-to-one correspondence of proton flux. The associated transverse mode can be regarded as Alfvén waves coupled with magnetosonic waves, as in the terrestrial magnetosphere. However, in the low-beta magnetosphere ($\beta < 1$), the slow magnetosonic waves have a phase speed on the same order of ion thermal speed, which indicates that the waves will be damped via Landau damping (Southwood & Hughes, 1983). The observed long-life waves do not agree with the theoretical expectation. One possible explanation is that long-lasting drivers, such as KH waves at the magnetopause, continuously excite the ∼15 mHz waves(Liljeblad et al., 2016). For the mirror mode (or drift mirror waves), the particle is modulated via mirror effects. The modulation efficiency of the mirror mode waves depends on the anisotropy of plasma and the loss cone size of the magnetic bottle. This interpretation can be supported by the observed anisotropies in Figures 1f and 5f while further quantitative analysis is still required. Other candidates, including heavy ion cyclotron waves, are not considered here due to insufficient observation. Apart from compressional waves, the transverse components are also notable. However, they are highly coherent the compressional waves. And, the one-to-one correspondences between the transverse modes and proton flux are not as compatible as that between the compressional mode and proton flux. So, we cannot determine what roles do they play in this event.

Compared to the ULF wave-particle modulation on Earth, the large amplitude (relative to the ambient field) long-period compressional ULF waves are capable of causing a more substantial mirror effect. This effect could be signified by the large ratio of proton flux maximum and minimum. On the other hand, the relatively large amplitude also suggests the presence of the non-linear growth stage of the wave development. The apparent asymmetric wave peaks and dips in Case I could be one of the pieces of evidence for the above inference. Besides, resonant modulations (e.g., bounce resonance, drift resonance) are essential in explaining the wave-particle modulation on Earth. Nevertheless, there is no clear energy dependence or pitch angle dependence of the modulation shown in the present observation.

The ∼1 Hz waves observed in these events have similar characteristics to the waves reported by C. Russell et al. (1988) and Boardsen et al. (2009). Previous interpretations of these waves include ion-ion hybrid waves (for the transverse dominant waves) and electromagnetic ion Bernstein mode waves (for the compressional dominant waves at lower magnetic latitudes). In this case, both compressional dominant and transverse dominant waves are observed between 10° S and 40° N magnetic latitude. So, the observed waves are possible a mixture of two kinds of waves. The compressibility and power of these waves are overall higher near the magnetic equator than at higher latitudes, coinciding with the previous statistics and theoretical interpretations. Apart from the latitudinal difference, the ∼1 Hz wave power and compressibility have an additional periodic variation with periods of long-period ULF waves. This periodicity suggests the ∼1Hz waves may be modulated by the long period compressional ULF waves via the changes in plasma flux (or pressure) since the plasma beta may influence the growth of plasma instability and mode conversion of waves. The unchanged ∼ 1Hz wave frequency implies that the excitation and modulation of the ∼1 Hz waves might not occur locally, unlike the modulation on proton flux. This possibility is also supported by the statistical fact that the

proton flux modulation and high-frequency wave modulation are not always observed together. However, these deductions still have large uncertainty based on the existing observations. Several parameters (e.g., heavy ion density, plasma beta, ion perpendicular and parallel temperatures) are also crucial to the excitation of ion-ion hybrid waves and ion Bernstein mode waves. They may also be determinative in the wave-wave modulation and are not considered at the present stage(Denton et al., 2010; Kim et al., 2016). The charged particle and electromagnetic field instruments onboard BepiColombo are also expected to unveil nature of these waves furtherly(Benkhoff et al., 2021)

This paper can be summarized as follows:

1. Our observations confirm that ∼15 mHz compressional waves can modulate proton flux significantly.

2. Large amplitudes out-of-phase one-to-one correlations between the magnetic field intensity and proton flux indicates that ULF waves control the plasma environment.

3. The ∼1 Hz coherent wave power and compressibility observed during the same interval are modulated by ∼15 mHz compressional waves. This modulation may be implemented via the changes in plasma flux, and it helps us better understand the ubiquitous ∼1 Hz waves in Mercury's magnetosphere.

Acknowledgments

This work was supported by the China Space Agency project (D020301 and D020303), the National Natural Science Foundation of China (42011530080, 41974191) and a research grant from the National Key R&D Program of China 2020YFE0202100. We are grateful to MESSENGER Magnetometer and Fast Imaging Plasma Spectrometer (FIPS) for providing the data. MESSENGER data used in this study were available from the Planetary Data System (PDS): `http://pds.jpl.nasa.gov`; Magnetometer: `https://pds-ppi.igpp.ucla.edu/search/view/?f=yes\&id=pds://PPI/MESS-E\_V\_H\_SW-MAG-3-CDR-CALIBRATED-V1.0` and Fast Imaging Plasma Spectrometer: `https://pds-ppi.igpp.ucla.edu/search/view/?f=yes\&id=pds://PPI/MESS-E\_V\_H\_SW-EPPS-3-FIPS-DDR-V2.0`.

References

Alexeev, I. I., Belenkaya, E. S., Slavin, J. A., Korth, H., Anderson, B. J., Baker, D. N., ... Solomon, S. C. (2010). Mercury's magnetospheric magnetic field after the first two messenger flybys. *Icarus*, *209*(1), 23 - 39. Retrieved from `http://www.sciencedirect.com/science/article/pii/S0019103510000436` (Mercury after Two MESSENGER Flybys) doi: https://doi.org/10.1016/j.icarus.2010.01.024

Anderson, B. J., Acuña, M. H., Lohr, D. A., Scheifele, J., Raval, A., Korth, H., & Slavin, J. A. (2007, Aug 01). The magnetometer instrument on messenger. *Space Science Reviews*, *131*(1), 417–450. Retrieved from `https://doi.org/10.1007/s11214-007-9246-7` doi: 10.1007/s11214-007-9246-7

Anderson, B. J., Johnson, C. L., Korth, H., Purucker, M. E., Winslow, R. M., Slavin, J. A., ... Zurbuchen, T. H. (2011). The global magnetic field of mercury from messenger orbital observations. *Science*, *333*(6051), 1859–1862. Retrieved from `http://science.sciencemag.org/content/333/6051/1859` doi: 10.1126/science.1211001

Anderson, B. J., Johnson, C. L., Korth, H., Winslow, R. M., Borovsky, J. E., Purucker, M. E., ... McNutt Jr., R. L. (2012). Low-degree structure in mercury's planetary magnetic field. *Journal of Geophysical Research: Planets*, *117*(E12). Retrieved from `https://agupubs.onlinelibrary.wiley.com/doi/abs/10.1029/2012JE004159` doi: 10.1029/2012JE004159

Andrews, G. B., Zurbuchen, T. H., Mauk, B. H., Malcom, H., Fisk, L. A., Gloeckler, G., ... Raines, J. M. (2007, Aug 01). The energetic particle and plasma spectrometer instrument on the messenger spacecraft. *Space Science Reviews*, *131*(1), 523–556. Retrieved from https://doi.org/10.1007/s11214-007-9272-5 doi: 10.1007/s11214-007-9272-5

Boardsen, S. A., Anderson, B. J., Acuña, M. H., Slavin, J. A., Korth, H., & Solomon, S. C. (2009). Narrow-band ultra-low-frequency wave observations by messenger during its january 2008 flyby through mercury's magnetosphere. *Geophysical Research Letters*, *36*(1). Retrieved from https://agupubs.onlinelibrary.wiley.com/doi/abs/10.1029/2008GL036034 doi: https://doi.org/10.1029/2008GL036034

Boardsen, S. A., Kim, E.-H., Raines, J. M., Slavin, J. A., Gershman, D. J., Anderson, B. J., ... Travnicek, P. (2015). Interpreting 1 hz magnetic compressional waves in mercury's inner magnetosphere in terms of propagating ion-bernstein waves. *Journal of Geophysical Research: Space Physics*, *120*(6), 4213-4228. Retrieved from https://agupubs.onlinelibrary.wiley.com/doi/abs/10.1002/2014JA020910 doi: https://doi.org/10.1002/2014JA020910

Boardsen, S. A., Slavin, J. A., Anderson, B. J., Korth, H., Schriver, D., & Solomon, S. C. (2012). Survey of coherent ∼1 hz waves in mercury's inner magnetosphere from messenger observations. *Journal of Geophysical Research: Space Physics*, *117*(A12). Retrieved from https://agupubs.onlinelibrary.wiley.com/doi/abs/10.1029/2012JA017822 doi: https://doi.org/10.1029/2012JA017822

Boardsen, S. A., Sundberg, T., Slavin, J. A., Anderson, B. J., Korth, H., Solomon, S. C., & Blomberg, L. G. (2010). Observations of kelvin-helmholtz waves along the dusk-side boundary of mercury's magnetosphere during messenger's third flyby. *Geophysical Research Letters*, *37*(12). Retrieved from https://agupubs.onlinelibrary.wiley.com/doi/abs/10.1029/2010GL043606 doi: https://doi.org/10.1029/2010GL043606

Denton, R. E., Engebretson, M. J., Keiling, A., Walsh, A. P., Gary, S. P., Décréau, P. M. E., ... Rème, H. (2010). Multiple harmonic ulf waves in the plasma sheet boundary layer: Instability analysis. *Journal of Geophysical Research: Space Physics*, *115*(A12). Retrieved from https://agupubs.onlinelibrary.wiley.com/doi/abs/10.1029/2010JA015928 doi: https://doi.org/10.1029/2010JA015928

DiBraccio, G. A., Slavin, J. A., Raines, J. M., Gershman, D. J., Tracy, P. J., Boardsen, S. A., ... Solomon, S. C. (2015). First observations of mercury's plasma mantle by messenger. *Geophysical Research Letters*, *42*(22), 9666-9675. Retrieved from https://agupubs.onlinelibrary.wiley.com/doi/abs/10.1002/2015GL065805 doi: 10.1002/2015GL065805

Elkington, S. R., Hudson, M. K., & Chan, A. A. (2003). Resonant acceleration and diffusion of outer zone electrons in an asymmetric geomagnetic field. *Journal of Geophysical Research: Space Physics*, *108*(A3). Retrieved from https://agupubs.onlinelibrary.wiley.com/doi/abs/10.1029/2001JA009202 doi: https://doi.org/10.1029/2001JA009202

Gershman, D. J., Slavin, J. A., Raines, J. M., Zurbuchen, T. H., Anderson, B. J., Korth, H., ... Solomon, S. C. (2014). Ion kinetic properties in mercury's pre-midnight plasma sheet. *Geophysical Research Letters*, *41*(16), 5740-5747. Retrieved from https://agupubs.onlinelibrary.wiley.com/doi/abs/10.1002/2014GL060468 doi: 10.1002/2014GL060468

Imber, S. M., & Slavin, J. A. (2017). Messenger observations of magnetotail loading and unloading: Implications for substorms at mercury. *Journal of Geophysical Research: Space Physics*, *122*(11), 11,402-11,412. Retrieved from https://agupubs.onlinelibrary.wiley.com/doi/abs/10.1002/2017JA024332 doi: 10.1002/2017JA024332

Jacobs, J., & Westphal, K. (1964). Geomagnetic micropulsations. *Physics and Chemistry of the Earth*, *5*, 157-224. Retrieved from https://www.sciencedirect.com/science/article/pii/S0079194664800057 doi: https://doi.org/10.1016/S0079-1946(64)80005-7

James, M. K., Imber, S. M., Yeoman, T. K., & Bunce, E. J. (2019). Field line resonance in the hermean magnetosphere: Structure and implications for plasma distribution. *Journal of Geophysical Research: Space Physics*, *124*(1), 211-228. Retrieved from https://agupubs.onlinelibrary.wiley.com/doi/abs/10.1029/2018JA025920 doi: https://doi.org/10.1029/2018JA025920

Kim, E.-H., Boardsen, S. A., Johnson, J. R., & Slavin, J. A. (2016). Ulf waves at mercury. In *Low-frequency waves in space plasmas* (p. 323-341). American Geophysical Union (AGU). Retrieved from https://agupubs.onlinelibrary.wiley.com/doi/abs/10.1002/9781119055006.ch19 doi: https://doi.org/10.1002/9781119055006.ch19

Liljeblad, E., Karlsson, T., Sundberg, T., & Kullen, A. (2016). Observations of magnetospheric ulf waves in connection with the kelvin-helmholtz instability at mercury. *Journal of Geophysical Research: Space Physics*, *121*(9), 8576-8588. Retrieved from https://agupubs.onlinelibrary.wiley.com/doi/abs/10.1002/2016JA023015 doi: https://doi.org/10.1002/2016JA023015

Liu, S., Xia, Z., Chen, L., Liu, Y., Liao, Z., & Zhu, H. (2019). Magnetospheric multiscale observation of quasiperiodic emic waves associated with enhanced solar wind pressure. *Geophysical Research Letters*, *46*(13), 7096-7104. Retrieved from https://agupubs.onlinelibrary.wiley.com/doi/abs/10.1029/2019GL083421 doi: https://doi.org/10.1029/2019GL083421

Liu, Z.-Y., Zong, Q.-G., Zhou, X.-Z., Zhu, Y.-F., & Gu, S.-J. (2020). Pitch angle structures of ring current ions induced by evolving poloidal ultra-low frequency waves. *Geophysical Research Letters*, *47*(4), e2020GL087203. Retrieved from https://agupubs.onlinelibrary.wiley.com/doi/abs/10.1029/2020GL087203 (e2020GL087203 10.1029/2020GL087203) doi: https://doi.org/10.1029/2020GL087203

Loto'aniu, T. M., Singer, H. J., Waters, C. L., Angelopoulos, V., Mann, I. R., Elkington, S. R., & Bonnell, J. W. (2010). Relativistic electron loss due to ultralow frequency waves and enhanced outward radial diffusion. *Journal of Geophysical Research: Space Physics*, *115*(A12). Retrieved from https://agupubs.onlinelibrary.wiley.com/doi/abs/10.1029/2010JA015755 doi: https://doi.org/10.1029/2010JA015755

Philpott, L. C., Johnson, C. L., Anderson, B. J., & Winslow, R. M. (2020). The shape of mercury's magnetopause: The picture from messenger magnetometer observations and future prospects for bepicolombo. *Journal of Geophysical Research: Space Physics*, *125*(5), e2019JA027544. Retrieved from https://agupubs.onlinelibrary.wiley.com/doi/abs/10.1029/2019JA027544 (e2019JA027544 10.1029/2019JA027544) doi: https://doi.org/10.1029/2019JA027544

Raines, J. M., Slavin, J. A., Zurbuchen, T. H., Gloeckler, G., Anderson, B. J., Baker, D. N., ... McNutt, R. L. (2011). Messenger observations of the plasma environment near mercury. *Planetary and Space Science*, *59*(15), 2004 - 2015. Retrieved from http://www.sciencedirect.com/science/article/pii/S0032063311000547 (Mercury after the MESSENGER flybys) doi: https://doi.org/10.1016/j.pss.2011.02.004

Russell, C., Baker, D., & Slavin, J. (1988). The magnetosphere of mercury. *Mercury*, 514–561.

Russell, C. T. (1989). Ulf waves in the mercury magnetosphere. *Geophysical Research Letters*, *16*(11), 1253-1256. Retrieved from https://agupubs.onlinelibrary.wiley.com/doi/abs/10.1029/GL016i011p01253 doi: https://doi.org/10.1029/GL016i011p01253

Rönnmark, K., & André, M. (1991). Convection of ion cyclotron waves to ion-heating regions. *Journal of Geophysical Research: Space Physics*, *96*(A10), 17573-17579. Retrieved from https://agupubs.onlinelibrary.wiley.com/doi/abs/10.1029/91JA01793 doi: https://doi.org/10.1029/91JA01793

Santolík, O., Parrot, M., & Lefeuvre, F. (2003). Singular value decomposition methods for wave propagation analysis. *Radio Science*, *38*(1). Retrieved from https://agupubs.onlinelibrary.wiley.com/doi/abs/10.1029/2000RS002523 doi: https://doi.org/10.1029/2000RS002523

Slavin, J. A., Acuña, M. H., Anderson, B. J., Baker, D. N., Benna, M., Boardsen, S. A., ... Zurbuchen, T. H. (2009). Messenger observations of magnetic reconnection in mercury's magnetosphere. *Science*, *324*(5927), 606–610. Retrieved from http://science.sciencemag.org/content/324/5927/606 doi: 10.1126/science.1172011

Southwood, D. J., & Hughes, W. J. (1983). Theory of hydromagnetic waves in the magnetosphere [Journal Article]. *Space Science Reviews*, *35*(4), 301-366. Retrieved from https://doi.org/10.1007/BF00169231 doi: 10.1007/BF00169231

Sun, W.-J., Slavin, J. A., Fu, S., Raines, J. M., Sundberg, T., Zong, Q.-G., ... Zurbuchen, T. H. (2015). Messenger observations of alfvénic and compressional waves during mercury's substorms. *Geophysical Research Letters*, *42*(15), 6189-6198. Retrieved from https://agupubs.onlinelibrary.wiley.com/doi/abs/10.1002/2015GL065452 doi: 10.1002/2015GL065452

Sun, W.-J., Slavin, J. A., Fu, S., Raines, J. M., Zong, Q.-G., Imber, S. M., ... Baker, D. N. (2015). Messenger observations of magnetospheric substorm activity in mercury's near magnetotail. *Geophysical Research Letters*, *42*(10), 3692-3699. Retrieved from https://agupubs.onlinelibrary.wiley.com/doi/abs/10.1002/2015GL064052 doi: 10.1002/2015GL064052

Sundberg, T., Boardsen, S. A., Slavin, J. A., Anderson, B. J., Korth, H., Zurbuchen, T. H., ... Solomon, S. C. (2012). Messenger orbital observations of large-amplitude kelvin-helmholtz waves at mercury's magnetopause. *Journal of Geophysical Research: Space Physics*, *117*(A4). Retrieved from https://agupubs.onlinelibrary.wiley.com/doi/abs/10.1029/2011JA017268 doi: 10.1029/2011JA017268

Winslow, R. M., Anderson, B. J., Johnson, C. L., Slavin, J. A., Korth, H., Purucker, M. E., ... Solomon, S. C. (2013). Mercury's magnetopause and bow shock from messenger magnetometer observations. *Journal of Geophysical Research: Space Physics*, *118*(5), 2213-2227. Retrieved from https://agupubs.onlinelibrary.wiley.com/doi/abs/10.1002/jgra.50237 doi: 10.1002/jgra.50237

Yue, C., Li, W., Nishimura, Y., Zong, Q., Ma, Q., Bortnik, J., ... Nicolls, M. J. (2016). Rapid enhancement of low-energy (<100 ev) ion flux in response to interplanetary shocks based on two van allen probes case studies: Implications for source regions and heating mechanisms. *Journal of Geophysical Research: Space Physics*, *121*(7), 6430-6443. Retrieved from https://agupubs.onlinelibrary.wiley.com/doi/abs/10.1002/2016JA022808 doi: https://doi.org/10.1002/2016JA022808

Zhao, J. T., Sun, W.-J., Zong, Q. G., Slavin, J. A., Zhou, X. Z., Dewey, R. M., ... Raines, J. M. (2019). A statistical study of the force balance and structure in the flux ropes in mercury's magnetotail. *Journal of Geophysical Research: Space Physics*, *124*(7), 5143-5157. Retrieved from https://agupubs.onlinelibrary.wiley.com/doi/abs/10.1029/2018JA026329 doi: 10.1029/2018JA026329

Zhao, J. T., Zong, Q. G., Yue, C., Sun, W. J., Zhang, H., Zhou, X. Z., ... Wei, Y. (2022). Observational evidence of ring current in the magnetosphere of mercury [Journal Article]. *Nat Commun*, *13*(1), 924. doi:

10.1038/s41467-022-28521-3

Zong, Q., Rankin, R., & Zhou, X. (2017). The interaction of ultra-low-frequency pc3-5 waves with charged particles in earth's magnetosphere [Journal Article]. *Reviews of Modern Plasma Physics*, *1*(1), 10. Retrieved from `https://doi.org/10.1007/s41614-017-0011-4` doi: 10.1007/s41614-017-0011-4

Zong, Q.-G., Zhou, X.-Z., Wang, Y. F., Li, X., Song, P., Baker, D. N., ... Pedersen, A. (2009). Energetic electron response to ulf waves induced by interplanetary shocks in the outer radiation belt. *Journal of Geophysical Research: Space Physics*, *114*(A10). Retrieved from `https://agupubs.onlinelibrary.wiley.com/doi/abs/10.1029/2009JA014393` doi: https://doi.org/10.1029/2009JA014393

Benkhoff, J., Murakami, G., Baumjohann, W., Besse, S., Bunce, E., Casale, M., ... Zender, J. (2021, Dec). Bepicolombo - mission overview and science goals. *Space Science Reviews*, *217*(8), 90. doi: 10.1007/s11214-021-00861-4

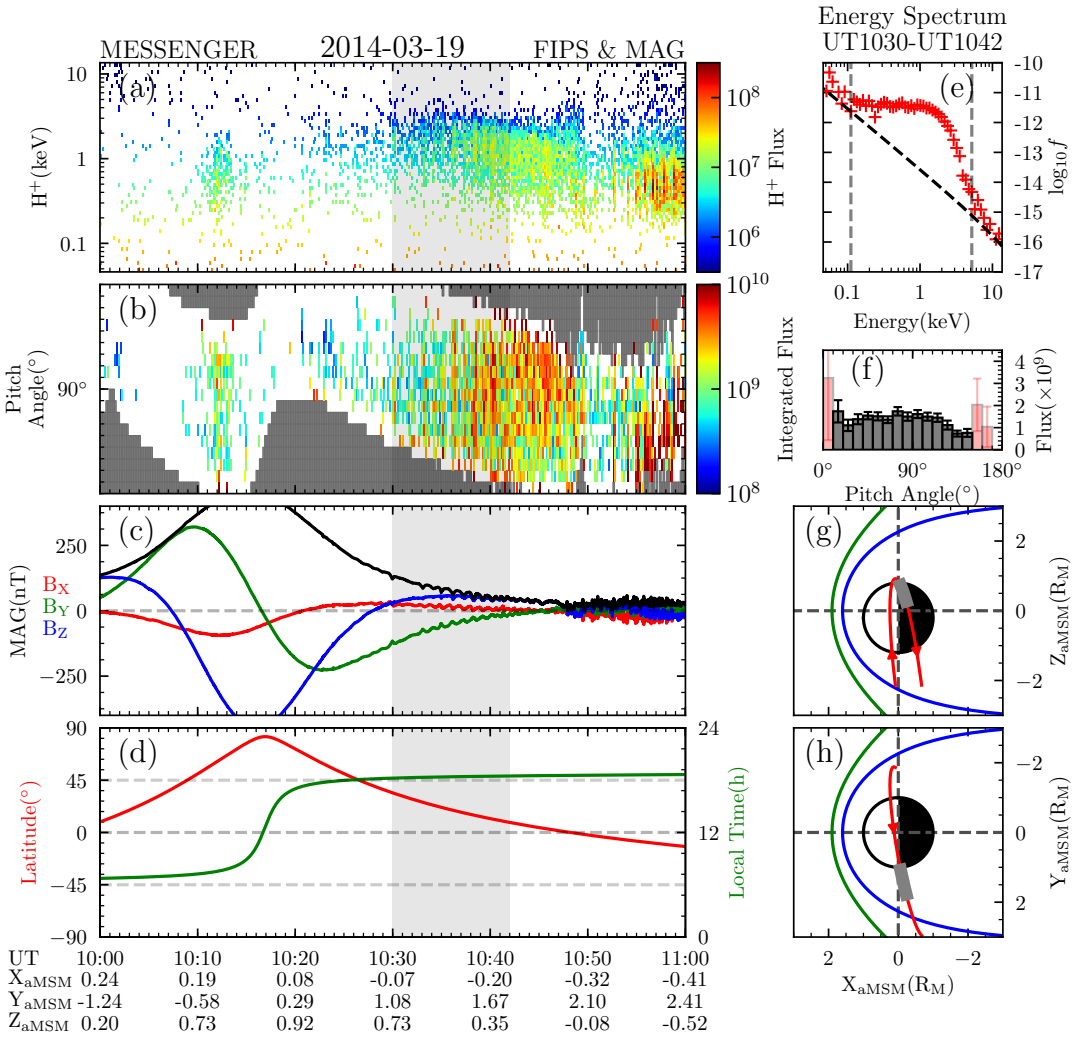

Figure 1. An overview of the ultra-low frequency pulsations event on 19th March, 2014 observed by MESSENGER's MAG and FIPS. (a) Differential number flux (in the unit of $cm^{-2} \cdot s^{-1} \cdot (keV/e)^{-1} \cdot sr^{-1}$) of protons measured by FIPS. (b) Pitch angle distribution (in the unit of $cm^{-2} \cdot s^{-1} \cdot sr^{-1}$). The pitch angle bins out of the field-of-view are filled with dark gray. (c) Magnetic field components (solid red, green, and blue lines for B_x, B_y and B_z) and intensity (solid black line). (d) Magnetic latitude and local time of the spacecraft. (e) The average energy spectrum of protons within the duration from UT 10:30 to UT 10:42. (f) Average pitch angle spectrum of protons within the duration from UT 10:30 to UT 10:42. Errorbars here are the standard errors of the mean. Pitch angle bins with large relative uncertainty (>50%) are marked with red color. (g, h) Trajectories of the spacecraft in the XY, XZ planes. The interval of interest is marked by the light gray shaded area in panels a-d and bold gray line in panels f-g. Universal time and spacecraft location in aMSM coordinate are presented at the bottom of the figure.

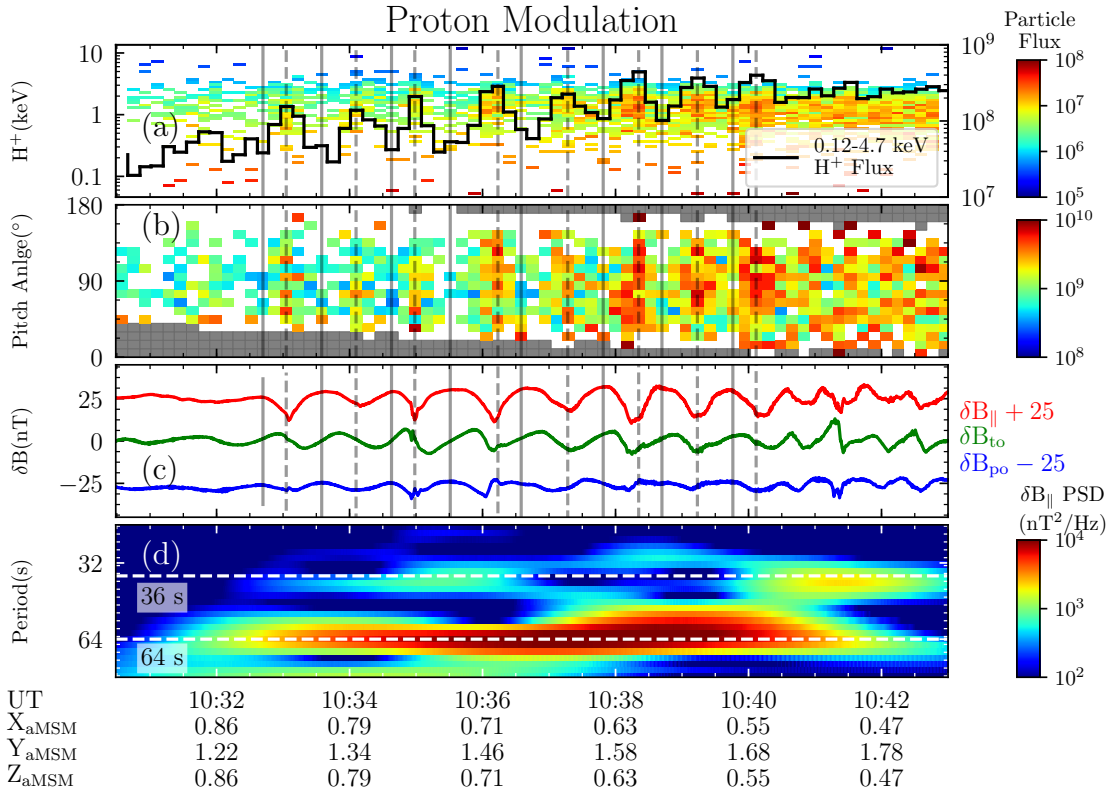

Figure 2. Proton modulation by ∼15 mHz compressional ULF waves. (a) The differential number flux of the proton (in the unit of $cm^{-2} \cdot s^{-1} \cdot (keV/e)^{-1} \cdot sr^{-1}$). The integrated flux of 0.12 keV - 4.71 keV protons is presented as the solid black line (in the unit of $cm^{-2} \cdot s^{-1} \cdot sr^{-1}$). (b) Pitch angle distribution (in the unit of $cm^{-2} \cdot s^{-1} \cdot sr^{-1}$). (c) The magnetic field detrended from the 300 s moving average in the field-aligned coordinate system. (d) Wavelet spectrum of the compressional mode magnetic field pulsations. The dashed white line indicates the periods of 36 s and 64 s.

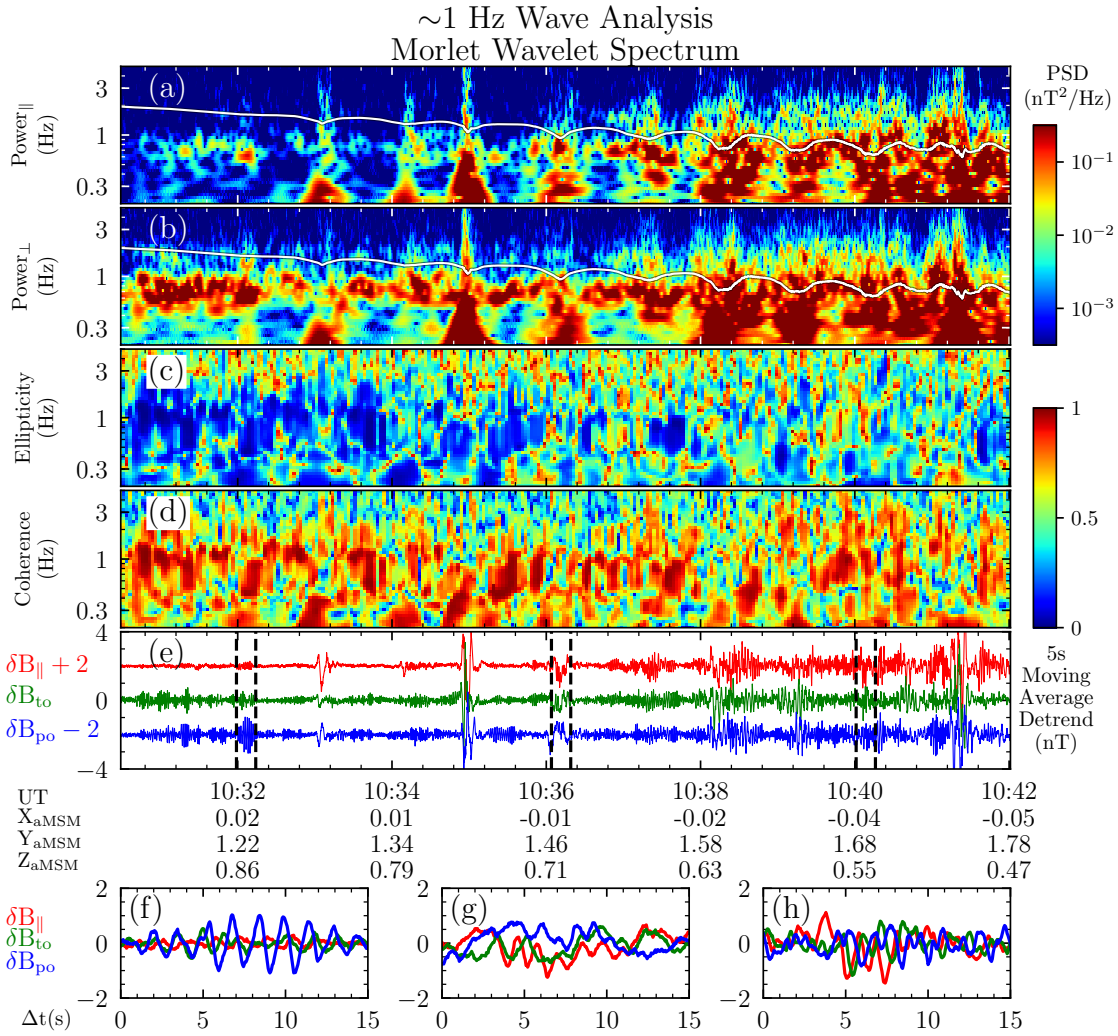

Figure 3. ~1 Hz coherent waves analysis. (a) Power spectrum of the compressional component, (b) and the transverse component. (c) Ellipticity. (d) Coherence. (e) The magnetic field waveform detrended from a 5 s moving average. (f, g, h) Three slices of ~1 Hz coherent waves with a detrended magnetic field. The time ranges of these three slices are marked as dashed black lines in panel e.

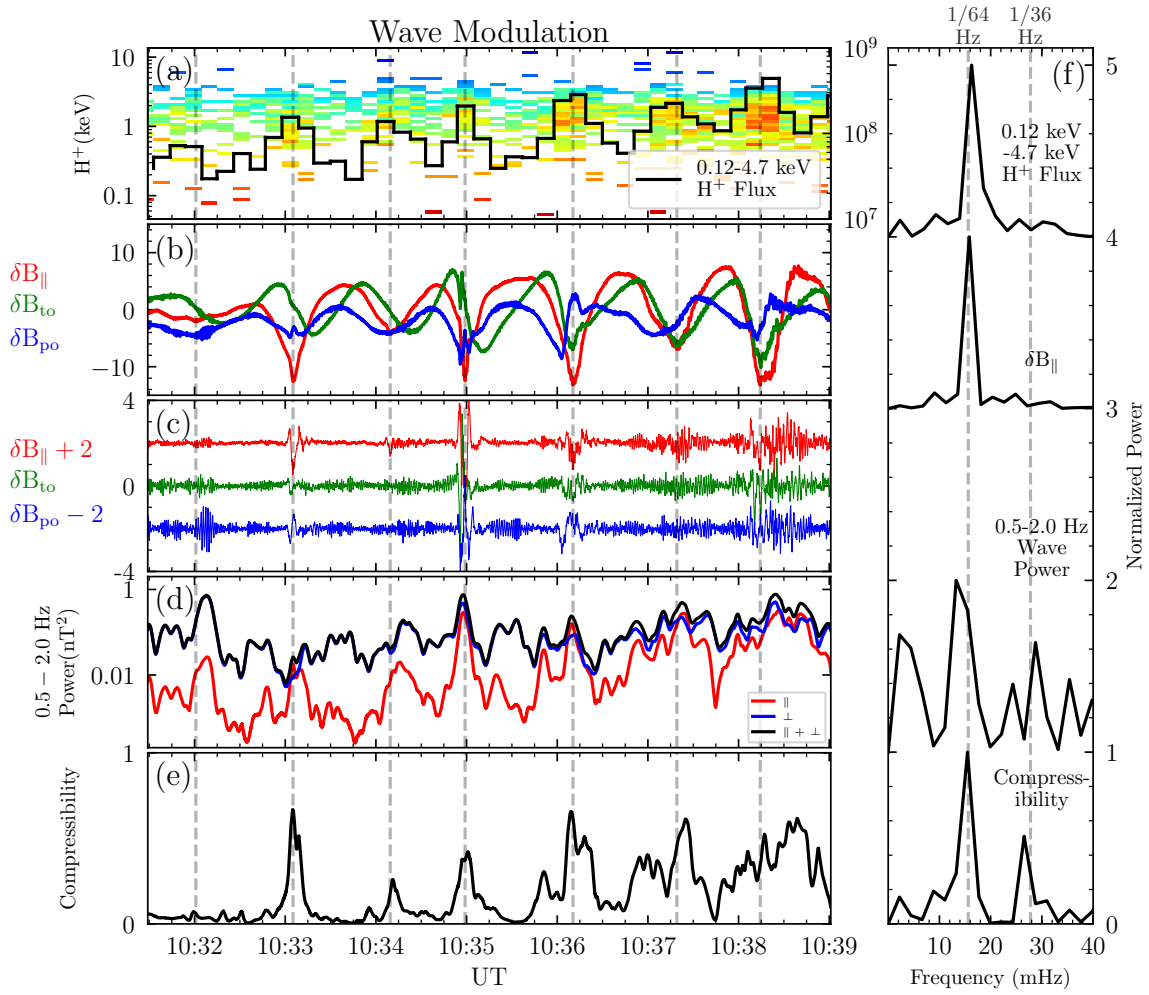

Figure 4. The one-to-one correspondence of ∼1 Hz waves and ∼15 mHz waves. (a) Proton spectrum adapted from Figure 2a. The solid black line displays the 0.12 keV to 4.7 keV proton flux. (b) The waveform of detrended ∼15 mHz waves. (c) The waveform of detrended ∼1 Hz waves. (d) 0.5-2.0 Hz integral wave power. (e) The ratio between 0.5-2.0 Hz integral compressional wave power and 0.5-2.0 Hz integral total wave power. (f) Discrete Fourier transform of 0.12 keV to 4.7 keV proton flux (solid black line in panel a), ∼15 mHz compressional waves (solid red line in panel b), integral wave power (solid black line in panel d), and compressibility (solid black line in panel e) of the ∼1 Hz waves.

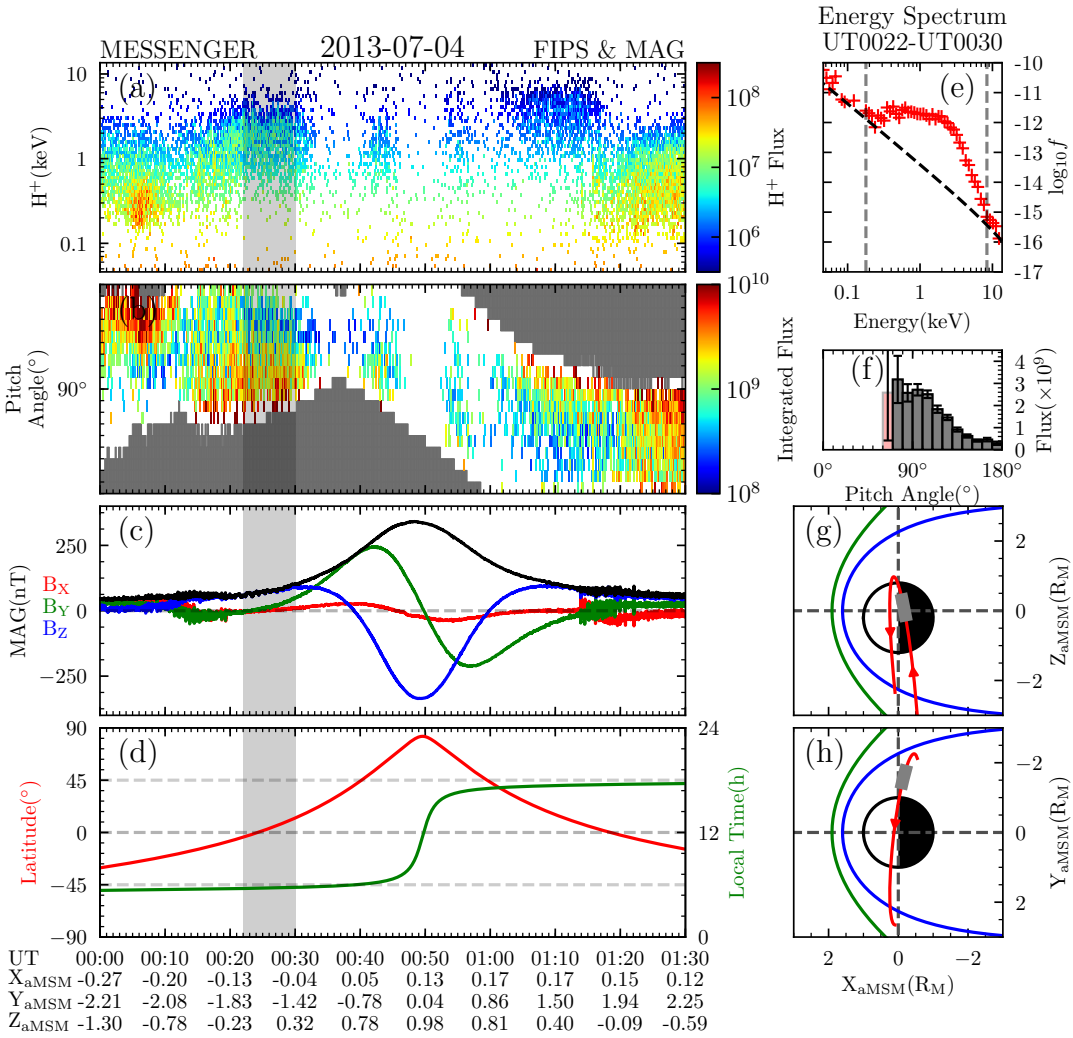

Figure 5. An overview of the ultra-low frequency pulsations event on 4th July, 2013 observed by MESSENGER's MAG and FIPS. (a) Differential number flux (in the unit of $cm^{-2} \cdot s^{-1} \cdot (keV/e)^{-1} \cdot sr^{-1}$) of protons measured by FIPS. (b) Pitch angle distribution (in the unit of $cm^{-2} \cdot s^{-1} \cdot sr^{-1}$). The pitch angle bins out of the field-of-view are filled with dark gray. (c) Magnetic field components (solid red, green, and blue lines for B_x, B_y and B_z) and intensity (solid black line). (d) Magnetic latitude and local time of the spacecraft. (e) The average energy spectrum of protons within the duration from UT 00:22 to UT 00:30. (f) Average pitch angle spectrum of protons within the duration from UT 00:22 to UT 00:30. Errorbars here are the standard errors of the mean. Pitch angle bins with large relative uncertainty (>50%) are marked with red color. (g, h) Trajectories of the spacecraft in the XY, XZ planes. The interval of interest is marked by the light gray shaded area in panels a-d and gray red line in panels f-g. Universal time and spacecraft location in aMSM coordinate are presented at the bottom of the figure.

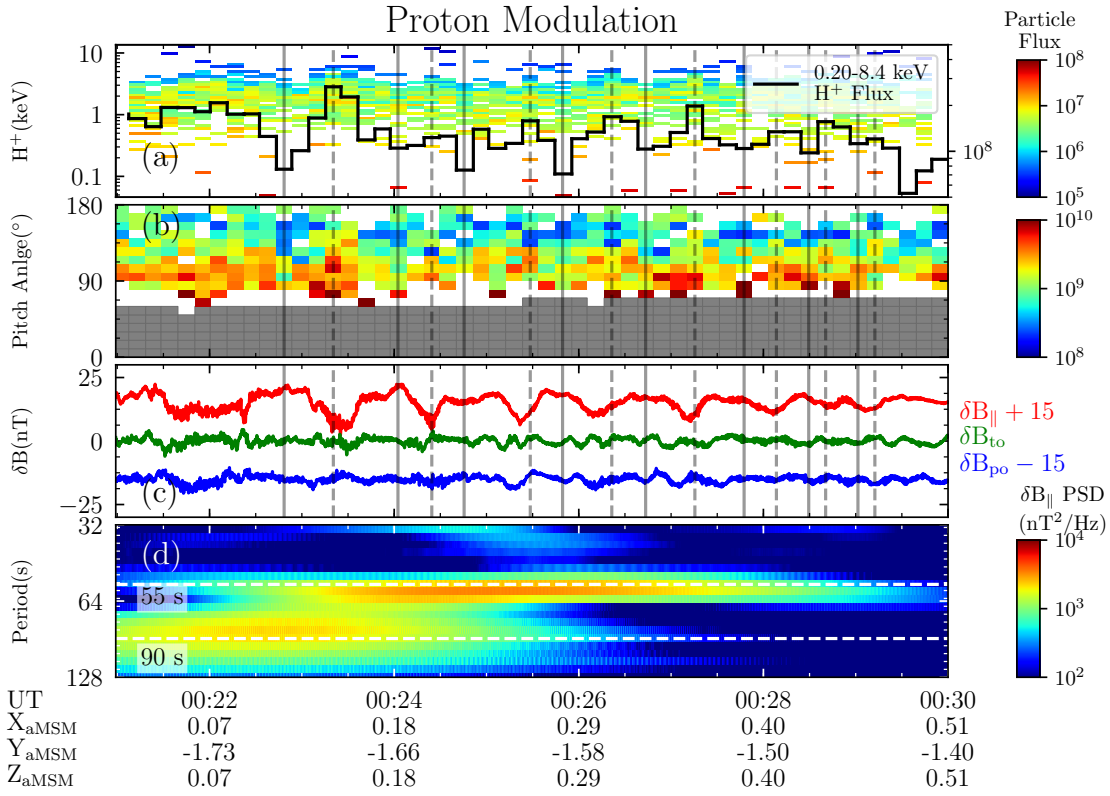

Figure 6. Proton modulation by ∼15 mHz compressional ULF waves. (a) The differential number flux of the proton (in the unit of $cm^{-2} \cdot s^{-1} \cdot (keV/e)^{-1} \cdot sr^{-1}$). The integrated flux of 0.20 keV - 8.4 keV protons is presented as the solid black line (in the unit of $cm^{-2} \cdot s^{-1} \cdot sr^{-1}$). (b) Pitch angle distribution (in the unit of $cm^{-2} \cdot s^{-1} \cdot sr^{-1}$). (c) The magnetic field detrended from the 300 s moving average in the field-aligned coordinate system. (d) Wavelet spectrum of the compressional mode magnetic field pulsations. The dashed white line indicates the periods of 55 s and 90 s.

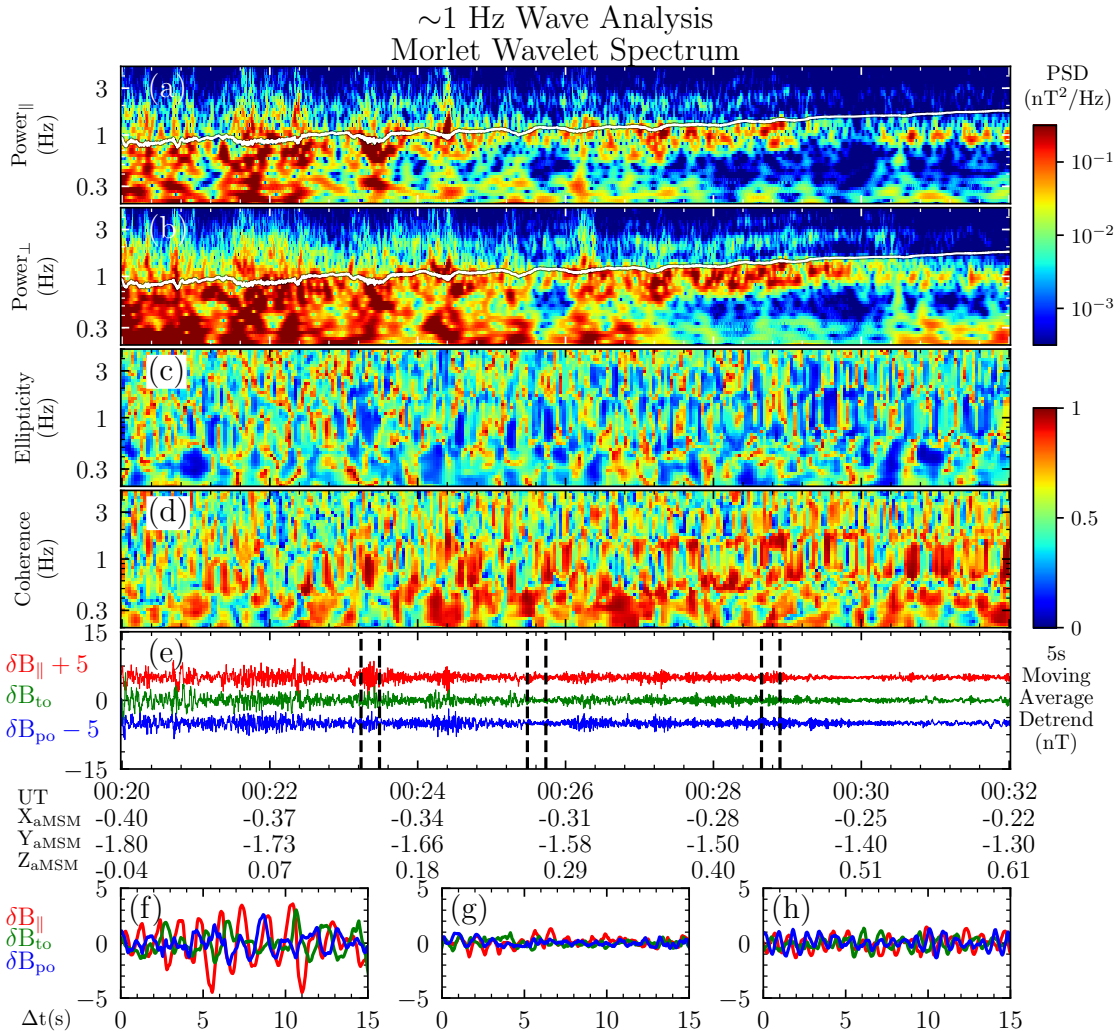

Figure 7. ~1 Hz coherent waves analysis. (a) Power spectrum of the compressional component, (b) and the transverse component. (c) Ellipticity. (d) Coherence. (e) The magnetic field waveform detrended from a 5 s moving average. (f, g, h) Three slices of ~1 Hz coherent waves with a detrended magnetic field. The time ranges of these three slices are marked as dashed black lines in panel e.

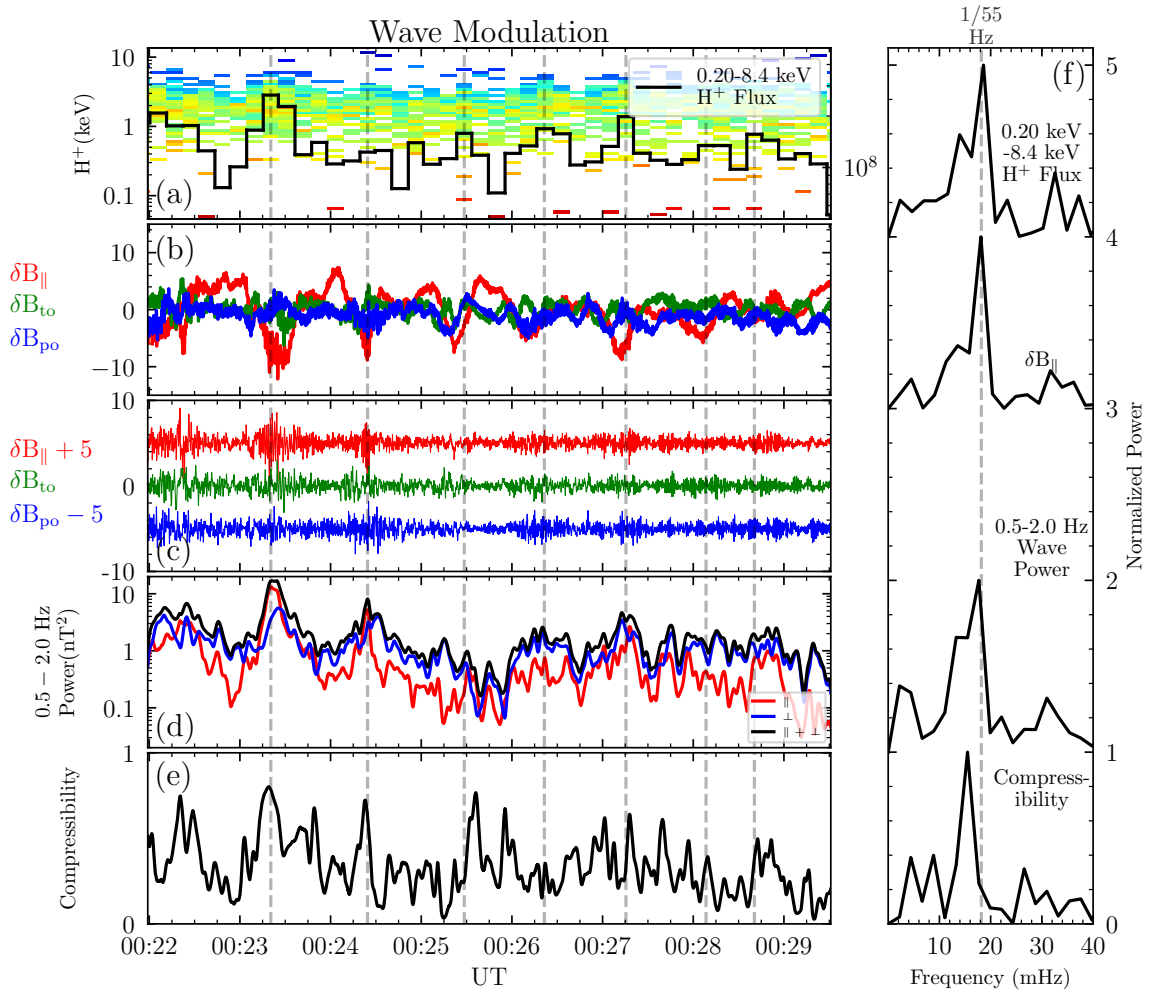

Figure 8. The one-to-one correspondence of ∼1 Hz waves and ∼15 mHz waves. (a) Proton spectrum adapted from Figure 6a. The solid black line displays the 0.20 keV to 8.4 keV proton flux. (b) The waveform of detrended ∼15 mHz waves. (c) The waveform of detrended ∼1 Hz waves. (d) 0.5-2.0 Hz integral wave power. (e) The ratio between 0.5-2.0 Hz integral compressional wave power and 0.5-2.0 Hz integral total wave power. (f) Discrete Fourier transform of 0.20 keV to 8.4 keV proton flux (solid black line in panel a), ∼15 mHz compressional waves (solid red line in panel b), integral wave power (solid black line in panel d), and compressibility (solid black line in panel e) of the ∼1 Hz waves.